Observation of singlet-triplet anticrossings in He

Terry A. Miller, Robert S. Freund, Foch Tsai,* Thomas J. Cook, and Bernard R. Zegarski
Bell Laboratories, Murray Hill, New Jersey 07974
(Received 19 February 1974)

Two independent anticrossings have been observed between singlet and triplet levels in the He atom, one between the $7\,^1D$ and $7\,^3D$ states, the other between the $8\,^1D$ and $8\,^3D$ states. The states are excited by electron bombardment. Compensatory changes in the luminosity of the singlet and triplet states are detected as the levels are tuned through the anticrossing points by a magnetic field. The positions of the anticrossings have been analyzed to provide new values for these singlet-triplet separations accurate to ~ 0.03 GHz. These results show the previous best optical determinations for the separations to be in error by over a GHz. The widths of the anticrossings are analyzed to provide the most direct measures of the spin-orbit coupling constant between a singlet and a triplet state yet obtained for any system. The measured values of these coupling constants are found to be several times larger than their corresponding diagonal value in the $7\,^3D$ and $8\,^3D$ states.

I. INTRODUCTION

The importance of singlet-triplet interactions in numerous areas of spectroscopy, laser development, and photochemistry is well known. In molecular spectroscopy, perturbations among states disrupt spectral regularity. Although it has often been difficult to identify precisely singlet-triplet perturbations, recent work[1] on CO seems to have gone far in this respect. Phosphoresence and intercombination lines and bands establish clearly singlet-triplet interaction. Numerous lasers are either assisted or inhibited by singlet-triplet transitions. Likewise, photochemical reactions are often influenced by singlet-triplet transitions.

The observance of any of the above effects, in some sense, constitutes a measurement of singlet-triplet interaction. However in no case is there a very direct measurement of either the relative positions of the singlet and triplet levels (except for intercombination lines and bands) or of the magnitude of the interaction between the singlet and triplet (i.e., the matrix element connecting the two). The experimental problem, of course, centers upon the relative weakness of the interaction between singlet and triplet levels along with the forbiddeness of transitions between them.

However, in some kinds of experiments quite forbidden interactions can be directly observed. Recently electric-field perturbations between excited atomic states of different parity have been observed[2,3] by the method of level anticrossing. Likewise, weak hyperfine perturbations have also been observed[4] by the anticrossing method. In these anticrossing experiments there exist energy levels in close proximity, but between which the perturbation is so small as to be scarcely noticeable in zero field. If, however, a (magnetic) field is used to tune these levels to essential degeneracy, the effect of even a small perturbation between the levels is no longer negligible.

According to the general Von Neumann[5] "noncrossing" rule, these levels must repel one another and avoid crossing. This avoided crossing or anticrossing may have a dramatic effect upon the luminosity of the decaying excited states. The details of this effect were first worked out by Wieder and Eck[4] and others[5-7] and later refined.[8,9] The relevant facets of the phenomenon are presented later in this paper, but in the simplest terms, luminosity is transferred from the more strongly radiating state to the less strongly radiating state. If the radiation of one of the anticrossing levels is selectively monitored as a function of field, the center of a sharp change in luminosity will mark the turning point for the anticrossing levels. Furthermore, the details of the theory show that both the intensity and width (in terms of magnetic field) of the effect are determined by the strength of the perturbation and the lifetimes of the states.

Based upon the above considerations, the desirability and possibility of observing anticrossings between excited singlet and triplet levels of light atoms and molecules seem apparent. Such observations would establish the relative positions of the singlet and triplet manifolds to an accuracy comparable to that of microwave spectroscopy. Also the width of the anticrossing should give the most *direct* measurement of the perturbation coupling a singlet and triplet level.

If one considers the He atom as an example, the possibility of the experimental observation of singlet-triplet anticrossings seems good. In moderately low rydberg states ($n \sim 5-10$) singlet-triplet separations of the D states lie in the GHz region. Such separations can easily be tuned to degeneracy by the application of moderate (kG)

magnetic fields and the perturbation between them may be even larger than in previous anticrossing experiments. These states decay with conveniently accessible and separable emissions in the visible and near uv spectral region. Finally they can be adequately and differentially populated by electron impact. Thus our choices for the initial singlet-triplet anticrossing experiments are the $n=7$ and 8 ^1D and ^3D states of He.

It is worthwhile recalling the recent experiments of Wing and Lamb[10] on the $n=7$ rydberg complex. They observed microwave transitions between the $n=7$ ^1D and $^{1,3}F$ (^1G and ^1H) levels and hence determined precise positions for these levels, i.e., the electrostatic fine structure. We will use certain of their results and we note that our experimental methods are not dissimilar to theirs. However, the singlet-triplet anticrossings which we observe represent a distinct physical phenomenon from the microwave transitions of their experiments and also have a quite different information content.

II. THEORY

A. Anticrossings

The basic theory describing the observable effects of two atomic levels undergoing an anticrossing as a function of field is given by Wieder and Eck.[4] Subsequent authors[8,9] have extended their treatment slightly to include excitation mechanisms other than optical pumping. The results of these theories can be summarized in the following equation governing the change of light output $I_{M,M'}$ of a pair of Zeeman levels of the excited atomic system near the point of anticrossing:

$$I_{M,M'}=\frac{2|V_{SM,TM'}|^2(\rho^0_{S,M}\tau_S-\rho^0_{T,M'}\tau_T)(K_{S,M}\tau_S-K_{T,M'}\tau_T)}{4|V_{SM,TM'}|^2(\tau_S\tau_T/\bar{\tau}^2)+\hbar^2\bar{\tau}^{-2}+g_e^2\mu_0^2(H-H_0)^2}, \tag{1}$$

where $V_{SM,TM'}$ is the matrix element of the perturbation between the Mth level of the singlet (S) state and the M'th level of the triplet (T) state; $\tau_{S(T)}$ is the lifetime of the singlet (triplet) state; $\rho^0_{S(T),M}$ is the diagonal element of the density matrix for the Mth level of the singlet (triplet) state; $K_{S(T),M}$ is the intensity of the emission of the Mth level of the singlet (triplet) state detected by the experimental apparatus; g_e is the effective g value between the two anticrossing levels; H_0 is the turning point of the levels in the avoided crossing; and $\bar{\tau}^{-1}=\frac{1}{2}(\tau_S^{-1}+\tau_T^{-1})$. Since experimentally one does not isolate a single Zeeman level in emission, one must sum the expression given above over all M and M' states. However, most of the important facets of the observed anticrossings are explicit in Eq. (1) even without the summation.

B. Singlet-triplet perturbation

Of the quantities in Eq. (1), perhaps the one most fundamental to the success of the experiment is the matrix element $V_{SM,TM'}$ of the perturbation between the singlet and triplet states. The only operator of reasonable magnitude that can connect a singlet and triplet state is the spin-orbit (and spin-other-orbit) operator. We can take the general form of this operator $\mathcal{H}_{SO}$ from the Breit equation,[11,12]

$$\mathcal{H}_{SO}=\frac{\mu_B}{mc}\left(\vec{\mathcal{E}}_1\times\vec{p}_1+\frac{2e}{r_{12}^3}(\vec{r}_{12}\times\vec{p}_2)\right)\cdot\vec{s}_1 + \frac{\mu_B}{mc}\left(\vec{\mathcal{E}}_2\times\vec{p}_2+\frac{2e}{r_{12}^3}(\vec{r}_{21}\times\vec{p}_1)\right)\cdot\vec{s}_2, \tag{2}$$

where the electric fields $\vec{\mathcal{E}}_1$ and $\vec{\mathcal{E}}_2$ are given, respectively, by

$$\vec{\mathcal{E}}_1=Z\vec{r}_1/r_1^3-\vec{r}_{12}/r_{12}^3, \tag{3}$$

$$\vec{\mathcal{E}}_2=Z\vec{r}_2/r_2^3-\vec{r}_{21}/r_{12}^3, \tag{4}$$

and the other symbols have their usual significance.

We can write $\mathcal{H}_{SO}$ in a particularly convenient form by introducing the operators

$$\vec{S}=\vec{s}_1+\vec{s}_2; \tag{5}$$

$$\vec{\mathcal{S}}=\vec{s}_1-\vec{s}_2. \tag{6}$$

Then $\mathcal{H}_{SO}$ can be rewritten

$$\begin{aligned}\mathcal{H}_{SO}=&\frac{\mu_B}{2mc}\left(\frac{Z\vec{l}_1}{r_1^3}+\frac{Z\vec{l}_2}{r_2^3}+\frac{3e}{r_{12}^3}[(\vec{r}_1\times\vec{p}_2)+(\vec{r}_2\times\vec{p}_1)-\vec{l}_1-\vec{l}_2]\right)\cdot\vec{S}\\ &+\frac{\mu_B}{2mc}\left(\frac{Z\vec{l}_1}{r_1^3}-\frac{Z\vec{l}_2}{r_2^3}+\frac{e}{r_{12}^3}[(\vec{r}_1\times\vec{p}_2)-(\vec{r}_2\times\vec{p}_1)+\vec{l}_1-\vec{l}_2]\right)\cdot\vec{\mathcal{S}}\\ =&A\vec{L}\cdot\vec{S}+\alpha\vec{L}\cdot\vec{\mathcal{S}},\end{aligned} \tag{7}$$

where $\vec{l}_{1(2)}$ is the orbital angular momentum of electron 1(2) and $\vec{L}=\vec{l}_1+\vec{l}_2$. The last line of Eq. (7) is obtained by the replacement theorem.[13] Formally A is to be equated to the first term within large parentheses in Eq. (7) multiplied by $[L(L+1)]^{-1/2}$, with an identical equation between $\mathcal{A}$ and the second term within large parentheses times $[L(L+1)]^{-1/2}$.

Equation (7) for $\mathcal{H}_{SO}$ is convenient in calculating the matrix elements $V_{SM,TM'}$. The term $A\vec{L}\cdot\vec{S}$ provides the diagonal spin-orbit coupling contribution to the fine structure of the triplet states. Its matrix elements, however, vanish between singlet and triplet states. On the other hand, the matrix elements of $\mathcal{A}\vec{L}\cdot\vec{s}$ vanish within a triplet state, but in general have nonzero values between singlet and triplet states. Thus we see that $V_{SM,TM'}$ is determined by $\mathcal{A}\vec{L}\cdot\vec{s}$ and is completely separable from the term $A\vec{L}\cdot\vec{S}$ that gives the diagonal fine structure. The actual matrix elements of $\mathcal{A}\vec{L}\cdot\vec{s}$ can be worked out by the methods of Condon and Shortley[14] or Racah.[15] We present these results for a ^3D and ^1D state in Table I.

C. He energy levels

1. *Zero field*

In order to interpret the experimental results, it is useful to consider what is already known about the structure of the $n=7$ and 8 rydberg states. There are, roughly speaking, three distinct kinds of structure. The largest splittings are the "electrostatic fine structure" separating the S, P, D, F, etc., states. The smallest splittings arise from the magnetic fine structure (spin-orbit and spin-spin coupling). The third structure is provided by the exchange energy which separates singlet and triplet states. For the S, P, and D states it is much larger than the magnetic fine structure and we can speak meaningfully about singlet and triplet levels. However, for F and higher states it is comparable to the magnetic fine structure and the spin-orbit–coupling-operator mixing makes the singlet and triplet designations not very meaningful.

TABLE I. Matrix elements $V_{SM,TM-1}$ of the operator $\mathcal{A}\vec{L}\cdot\vec{S}$. All the results listed below should be multiplied by the constant factor $\mathcal{A}(6)^{-1/2}$ to obtain the elements between a ^1D and a ^3D state. In all cases the M_S value is zero for the singlet and one for the triplet.

M_L	$V_{SM,TM-1}/[\mathcal{A}(6)^{-1/2}]$
2	$\sqrt{2}$
1	$\sqrt{3}$
0	$\sqrt{3}$
−1	$\sqrt{2}$
−2	0

The electrostatic structure is known for both the $n=7$ and 8 manifolds from optical spectroscopy.[16] For the 7 state these measurements are largely superseded by the much more accurate microwave work of Wing and Lamb.[10] The singlet-triplet separations in both the 7 and 8 states are known approximately from optical spectroscopy.[14] Some fine-structure measurements[10] have been carried out on the levels of the 7 state. Figure 1 is an energy-level diagram of the relevant portion of the $7d$ state based upon the best experimental data available. The magnetic fine structure is invisible on the scale of the diagram. The diagram for the 8 manifold is very similar except that all the splittings are compressed to about two-thirds those of the 7 states.

2. *First-order Zeeman effect*

Figure 1 also shows the effect of magnetic field upon the $n=7$ ^1D and ^3D energy levels. To a first approximation, the effect of the magnetic field is given by the linear Zeeman Hamiltonian

$$\mathcal{H}_1=\mu_B g_S\vec{H}\cdot\vec{S}+\mu_B g_L\vec{H}\cdot\vec{L}. \tag{8}$$

In terms of a decoupled representation (the com-

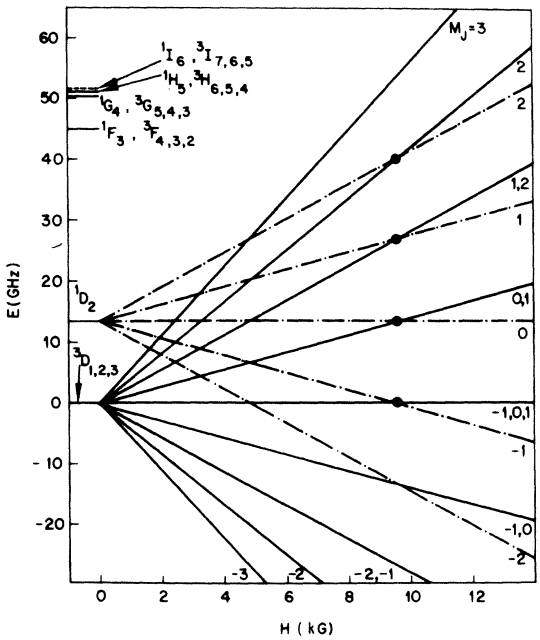

FIG. 1. Energy levels of helium with $n=7$ and $L\geq 2$. Zero-field energies are taken from Ref. 10, except for the positions of the ^3D and ^1D states, which are determined by this work. The four observable singlet-triplet anticrossings (which on the scale of the diagram occur at the same magnetic field) are indicated by large solid circles.

plete Paschen-Back effect) which is a sufficient approximation, the eigenvalues of $\mathcal{H}_1$ are just

$$\mathcal{H}_1 = \mu_B H(g_S M_S + g_L M_L). \tag{9}$$

In the above, g_S can be taken to be the free-electron spin g value. The g_L can be approximated by unity minus the correction for the finite nuclear mass,[17,18] giving $g_L = 1 - m/M = 0.999\,86$.

Consulting Table I and Fig. 1, we note that the only "crossing" levels of the ^1D and ^3D states with a nonzero perturbation between them are those of the ^1D state with quantum numbers $M_S = 0$, M_L, and those of the ^3D state with $M_S' = 1$ and $M_L' = M_L - 1$. Inserting these quantum numbers into Eq. (9) shows that the effective g value g_e for the anticrossings in Eq. (1) is just $g_L - g_S = -1.002\,46$ or $\mu_B g_e/h = -1.4030$ MHz/G. We also see that there are four such anticrossings with the singlet $M_L = 2$ to -1. In this approximation, the positions of all four anticrossings are precisely degenerate.

3. *Second-order effects*

Up to this point, we have discussed all the interactions which contribute to the energy levels depicted in Fig. 1 at a resolution appropriate to its scale. These interactions lead to the simple prediction of a four-fold degenerate anticrossing and have given an effective g value for it. There are, however, several terms which contribute effects invisibly small on the scale of Fig. 1 but not necessarily small compared to the precision of the present anticrossing experiment.

Let us call these terms second-order effects, since they are small in terms of energy magnitude though not necessarily second order in perturbation theory. There are three such terms. First there is the magnetic fine structure mentioned above and determined by the diagonal spin-orbit coupling constant A and the spin-spin coupling constant b. Second there is the quadratic Zeeman effect determined by the anisotropy of the diamagnetic susceptibility χ_A. Finally there is the second-order Stark effect determined by the product of the electric field ($\vec{\mathcal{F}}$), and the "off-diagonal" electric dipole moments ($\vec{\mu}$).

A general Hamiltonian encompassing these effects could be written

$$\mathcal{H}_2 = A\,\vec{L}\cdot\vec{S} + b\,\frac{3(\vec{L}\cdot\vec{S})^2 + \frac{3}{2}(\vec{L}\cdot\vec{S}) - \vec{L}^2\vec{S}^2}{2S(2S-1)L(2L-1)}$$

$$- \tfrac{1}{2}\chi_A T^2(\vec{H},\vec{H})\cdot T^2(\vec{L},\vec{L}) - \vec{\mathcal{F}}\cdot\vec{\mu}. \tag{10}$$

The first two terms of $\mathcal{H}_2$ are the standard form[19,20] for the magnetic fine-structure interactions. The next term describes the interaction of the magnetic field with the anisotropy of the magnetic susceptibility. This form has been given previously by Miller and Freund[18,21] without the factor of $\frac{1}{2}$. The omission of the $\frac{1}{2}$ in the earlier papers was an error; however, the matrix elements used in the computer program included this factor of $\frac{1}{2}$ and thus the previous results[18,21] for χ_A are all correct. The general form for χ_A is

$$\chi_A = \sum \frac{e^2}{4mc^2 L(2L-1)} \times \langle \eta L M_L = L | r^2(3\cos^2\theta - 1) | \eta L M_L = L \rangle, \tag{11}$$

where, for the $^{1,3}D$ states, $L = 2$. The final term describes the Stark interaction whose expectation value, of course, vanishes because of parity. However, the Stark effect is sufficiently large that second-order contributions must be considered.

The terms of $\mathcal{H}_2$ can be evaluated in the decoupled basis and there the diagonal terms are enough to adequately determine the energies. However, these diagonal terms depend on the atomic constants A, b, etc., which must be determined for the particular states. The expectation values of the first two terms vanish for the ^1D states so we have only to worry about the triplets. For the $7\,^3D$ state there are measurements[22,23] of the interval $J = 1 - J = 3 = \Delta\nu_{13} = 99.3$ MHz and $J = 2 - J = 3 = \Delta\nu_{23} = 7.3$ MHz. Evaluating the matrix elements of the first two terms of $\mathcal{H}_2$ in the coupled (zero-field) representation gives

$$\Delta\nu_{13} = \tfrac{5}{8}b - 5A, \tag{12}$$

$$\Delta\nu_{23} = -(3A - \tfrac{9}{8}b). \tag{13}$$

Solution of these equations with the measured intervals yields the values of A and b listed in Table II. These values in turn may be compared with the values of A and b calculated according to the hydrogenic approximation for rydberg states of He given by Bethe and Salpeter.[12] As can be

TABLE II. Values of A and b in the $7d$ and $8d\,^3D$ states. The experimental error limits are derived from the quoted uncertainties in the measurements of $\Delta\nu_{13}$ and $\Delta\nu_{23}$. The experimental values for the $8d$ state are the $7d$ experimental results multiplied by $(\frac{7}{8})^3$.

	$7d$		$8d$	
	Expt.[a]	Theory[b]	Expt.[c]	Theory[b]
A	-15.5 ± 3.2	-17.0	(-10.4 ± 2.1)	-11.4
b	34.8 ± 6.0	27.2	(23.3 ± 4.0)	18.3

[a] Derived from the results of Refs. 22 and 23.
[b] Reference 12.
[c] Extrapolated from $7d$ values.

seen from Table II, there is essential agreement between the theoretical and experimental numbers. This result is important, as there are no experimental measurements of the fine-structure intervals in the $8d\,^3D$ state. However, the closeness of the theoretical and experimental results for the $7d\,^3D$ state gives us confidence that we can obtain the $8d\,^3D$ results from theory. Thus under "experimental" in Table II we give the $7d$ results scaled by the appropriate rydberg factor,[12] $(\frac{7}{8})^3$. Under "theory" we give the direct theoretical calculation. The difference in the two results is negligible for our purposes.

For the quantity χ_A there are no experimental data for either the $7d$ or $8d\,^1D$ or ^3D states. Thus we turn again to the theory of Bethe and Salpeter to calculate χ_A. Since χ_A depends on an r^2 operator, whereas A and b depend on r^{-3}-type operators, the results for χ_A are likely to be more accurate than those for A and b. The results of these calculations are

$$\chi_A = -0.157 \text{ Hz/G}^2 \quad (7d\,^3D \text{ and } ^1D) \tag{14}$$

and

$$\chi_A = -0.274 \text{ Hz/G}^2 \quad (8d\,^3D \text{ and } ^1D). \tag{15}$$

Finally there is the Stark effect term. Once again, the hydrogenic approximation can be used to obtain the off-diagonal electric dipole moment. The electric field, however, arises from two sources. The first is the field derived from the presence of the electrons used to excite the He. This field would be very difficult to calculate. The problem has therefore been eliminated by extrapolating the position and breadth of the anticrossing line to zero electron current. However, this procedure does not eliminate the effects of the second electric field, the relativistic or motional electric field seen by the excited He atoms moving in the magnetic field. The magnitude of the electric field is given by[22]

$$\mathcal{F} = VH_0/c\,, \tag{16}$$

where V is the excited He's velocity perpendicular to $\vec{H}$ and H_0 is the anticrossing field. $\mathcal{F}$ is perpendicular to both $\vec{V}$ and $\vec{H}$. Ground-state He atoms are in thermal equilibrium at ~300 °K. The velocity distribution for the excited He atoms is unknown, but it seems unlikely to be very different from the ground state because of the low probability of momentum transfer in an electron-atom collision. Thus V can be taken[24] as the rms velocity $(2kT/m)^{1/2}$ of He atoms at 300 °K, which yields at the anticrossing fields

$$\mathcal{F} = 10.8 \text{ V/cm} \quad (7d\,^1D \text{ and } ^3D), \tag{17}$$

$$\mathcal{F} = 7.5 \text{ V/cm} \quad (8d\,^1D \text{ and } ^3D). \tag{18}$$

With the above values for the constants, $\mathcal{H}_2$ can be evaluated, but first the eigenvalues and second-order expressions must be obtained. These can be written

$$E_2 = AM_L M_S + b\left(\frac{3(M_L M_S)^2 + \frac{3}{2}(M_L M_S) - S(S+1)L(L+1)}{2S(2S-1)L(2L-1)}\right) - \frac{\chi_A H^2}{6}\left[3M_L^2 - L(L+1)\right] + \left(\frac{3\mathcal{F}nea_0}{4}\right)^2 (2L-1)^{-1}$$

$$\times\left[\frac{[n^2-(L+1)]^2}{2L+3}\left(\frac{(L+M+1)(L+M+2)}{^{1,3}E_{n,L,M_L} - {}^{1,3}E_{n,L+1,M_L+1}} + \frac{(L-M+1)(L-M+2)}{^{1,3}E_{n,L,M_L} - {}^{1,3}E_{n,L+1,M_L-1}}\right)\right]. \tag{19}$$

The expression E_2 is quite general and gives the second-order energies of all four states, $n = 7$ or 8 ^1D or ^3D. However, a few caveats must be honored to obtain these results simply. Firstly it should be remembered that the anticrossing levels are $^1D\,M_S = 0$, M_L and $^3D\,M_S = 1$, $M_L - 1$. Thus in all the calculations only the difference in E_2 for these pairs of states is important. The contributions from the first two terms of E_2 vanish for both ^1D states. The parameters A, b, $\mathcal{F}$, and χ_A are n dependent and the proper values from the text must be inserted for each state. In the last term $^{1,3}E_{n,L,M_L}$ denotes the actual, experimental energy of the singlet or triplet level of $n\,D$ with a given decoupled quantum number M_L (and the same M_S) including the effect of the term $\mathcal{H}_1$. This second-order expression only includes coupling to the F manifold; the coupling to the P manifold is much smaller.

Table III summarizes the calculated difference in energy using Eq. (19) for each pair (singlet minus triplet) of anticrossing levels. It is clear from Table III that E_2 removes the precise coincidence of the four anticrossings. Thus the presence of E_2 will cause both a slight broadening and a shift of the center position of the anticrossing.

III. EXPERIMENTAL

The anticrossing signal is governed by Eq. (1), which dictates the salient features of the experimental apparatus. Since the lifetimes τ_S and τ_T are comparable, the diagonal density-matrix elements must differ and at least one must be non-

TABLE III. Numerical values for the difference (singlet minus triplet in MHz) in the levels M_L, $M_S = 0$ of the singlet and $M_L - 1$, $M_S = 1$ of the triplet state at the anticrossing field. These values are derived from the energy E_2 and are computed from Eq. (19).

Singlet M_L	Quadratic Zeeman	Fine structure	Motional stark	Total
$7d$				
2	22.3	37.3	1.5	61.1
1	7.4	34.8	1.2	43.4
0	−7.4	15.0	1.2	8.8
−1	−22.3	−22.3	1.6	−43.0
$8d$				
2	18.8	25.0	2.6	46.4
1	6.2	23.3	2.1	31.6
0	−6.2	10.0	2.1	5.9
−1	−18.8	−14.9	2.7	−31.0

zero for observation of an anticrossing signal. This requirement can be fulfilled by electron-impact excitation of ground-state He, which more effectively populates the singlet level than the triplet. Moreover, light emitted by either the singlet or triplet must be preferentially detected. The wavelengths of the principal emissions of the $7d$ and $8d$ $^{1,3}D$ states are listed in Table IV. Table IV shows that the wavelengths are sufficiently different so that moderate dispersion in the detection system is sufficient to detect any singlet or triplet line with the complete exclusion of the other.

Two entirely independent apparatuses have been used to perform these experiments. This redundancy was useful to guarantee that the observations were in no way traceable to instrumental artifacts. One apparatus was the same as that used to observe microwave optical magnetic resonance induced by electrons (MOMRIE) in H_2 and He. The second apparatus was built especially for the anticrossing experiments.

As the MOMRIE apparatus has been described elsewhere,[18,21,25] we here describe only the modifications for the anticrossing experiments. The microwave power was turned off and the luminescence in the cavity was viewed through the light pipe described before. An interference filter (centered at 4031 Å, full width at half-maximum 10 Å) was available which, when tilted off-normal isolated the $7\ ^1D$-$2\ ^1P$ emission at 4009 Å. Preliminary experiments were performed with this filter, a lens, and a EMI 6256Q or EMI 9558Q photomultiplier.

TABLE IV. Wavelength in air of He transitions taken from Ref. 16.

Transition	Wavelength (Å)
$7\ ^3D \rightarrow 2\ ^3P$	3705.005
$7\ ^1D \rightarrow 2\ ^1P$	4009.268
$8\ ^3D \rightarrow 2\ ^3P$	3634.369
$8\ ^1D \rightarrow 2\ ^1P$	3926.534

The output of the photomultiplier was connected across a 5-kΩ load resistor to one of the inputs of a PAR 113 differential preamplifier. The dc level of the phototube was effectively balanced by a mV dc level applied to the other input of the PAR 113. The output of the PAR 113 was connected to a PDP-8E computer that repetitively swept the magnetic field and averaged the signal according to a software program written by ourselves.

The signal-to-noise ratio of the anticrossing observed while operating in this mode was sufficiently high that we deduced that one could observe the anticrossing using a lens system to image the light on the entrance slit of a Spex $\frac{3}{4}$ meter spectrometer, even though the light-gathering capability of this system was quite inferior to the interference filter system. Thus the spectrometer system was used to observe the anticrossing signals carried by each of the optical emissions listed in Table IV. The output from the photomultiplier (in this case always the 6256Q because of its lower dark current) was handled exactly as described above. Representative anticrossing signals carried by the $7d\ ^1D$ and ^3D lines are shown in Fig. 2.

The pressure of He in the cavity during the experiments was in the range of 1–10 mTorr as measured by a MKS capacitance manometer. Magnetic field measurements were made, as has been described previously,[18,21,25] with an NMR fluxmeter. Any time-constant effects present

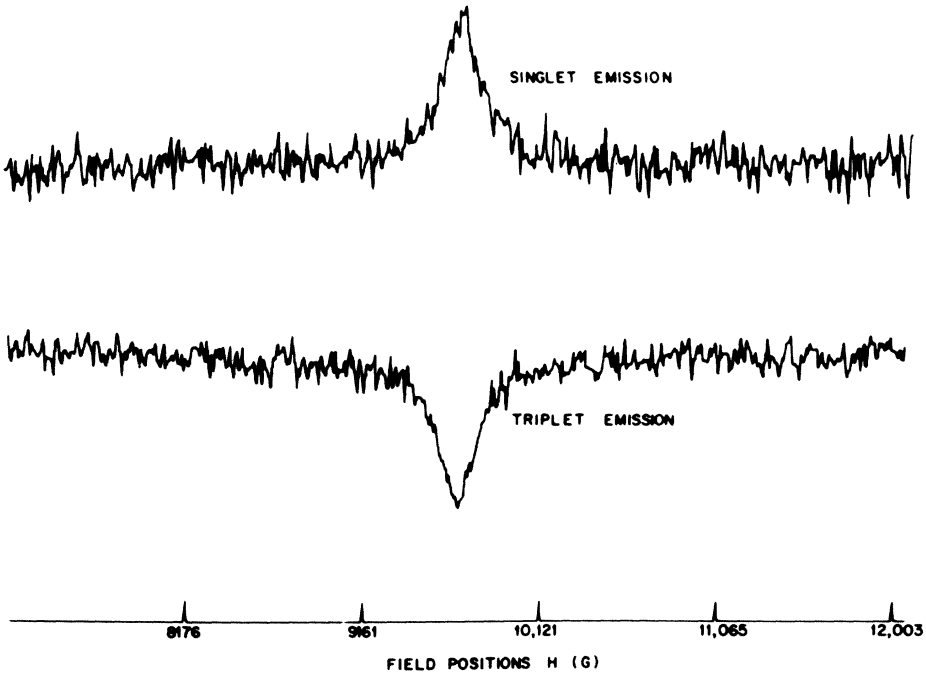

FIG. 2. Singlet and triplet anticrossing (blend 4 lines) as seen in the emission from the $7\,^1D$ state at 4009.3 Å and the $7\,^3D$ state at 3705.0 Å. Each of these runs was taken with the original (MOMRIE) apparatus and required 24 min of signal averaging with ~1 mTorr of helium and ~0.2 mA electron current.

in the averaging process were eliminated by combining measurements using increasing and decreasing magnetic-field sweeps.

Although ultimately the data obtained from the modified MOMRIE apparatus proved highly reliable, some initial problems raised doubts about its credibility. One of the problems was that a number of other lines similar to the singlet-triplet anticrossing were observed to be carried on the He luminescence, especially that from the singlet. Although most of these lines had no "mates" in the triplet luminescence, there were several weak features in the triplet luminescence in the same magnetic-field region. These "extra" lines decreased in intensity and narrowed much more rapidly than the singlet-triplet anticrossing as the electron current was decreased. Indeed, at low electron currents they disappeared entirely, as evidenced by Fig. 2. This behavior led us to believe that these lines were electric-field-induced anticrossings, perhaps involving other members of the $7d$ and $8d$ manifolds. However, using the available knowledge about these energy levels, we have not been able to uniquely assign these probable electric-field anticrossings.

The electric field postulated to account for these anticrossings arose from electron space charge in the cavity. Its presence had been established in other experiments and its most important component was known to lie perpendicular to the magnetic field. Besides possibly inducing electric-field anticrossings, it certainly Stark shifted and broadened the singlet-triplet anticrossing. Such a field, of course, must vanish if the electron current vanishes. Thus we extrapolated our results to zero electron current. However, since the exact dependence of the field upon current was unknown, the functional form of the extrapolation could only be guessed. Thus one could not be certain that a systematic error would not be included in the measurement.

Finally, the only observable characteristic of the singlet-triplet anticrossing was a change in luminosity as a function of magnetic field. Unfortunately, the magnetic field affects the trajectories of the electrons, an effect which under certain circumstances has been known to lead to broad undulations in luminosity as a function of magnetic field. While the details of these luminosity undulations were quite different from the anticrossing signal, it was impossible to absolutely eliminate the chance that the observed signal was an instrumental artifact.

For the reasons given above, it was felt that the anticrossing signal should be observed and measured in an independent apparatus as different as could be practical from the MOMRIE apparatus. A second apparatus was built with a different geometry and as small an electric field as possible. There was no microwave cavity, just an electron gun. The gun was quite different from that used in the MOMRIE apparatus and included a control grid. The cathode was of the same design as one previously described.[26] Its active

emitting surface (1×5 cm) was a nickel matrix filled with $BaSrCO_3$. It was supported (Fig. 3) on a quartz plate, along with a tungsten grid and anode. Mica spacers along the top and bottom edges separated the grid from the cathode by 0.5 mm. The grid-to-anode distance was about 5 mm. The anode and all electrical leads were supported by screws mounted in holes in the quartz plate.

The entire assembly was placed in a copper tee vacuum chamber previously described.[18] Copper tubing was wrapped around the exterior of the chamber for water cooling. The chamber was pumped by a combination Veeco pumping station and leak detector. The He luminosity was viewed with a light pipe passing through a quick-couple in the front flange of the chamber. Magnetic-field measurements were by means of the same NMR as with the other apparatus. The NMR probe extended into the vacuum chamber in a tube passing through a quick-couple in the top flange.

In a typical operation, He pressure in the chamber was in the mTorr region as estimated from the discharge gauge on the pumping station. An accelerating voltage of 30–50 V was maintained between the cathode and grid. Unfortunately, it was also found necessary to apply an additional 30–60 V between the grid and anode to obtain useable luminosity levels. Under these conditions, the total current collected at the anode was 50–100 mA. The current collected by the grid was about 10% of the anode value.

The He luminescence collected by the light pipe was isolated by the 4031-Å filter and monitored by a EMI 9558Q photomultiplier. The output of the phototube was connected to a 113 preamplifier and the computer, exactly as described above for the MOMRIE apparatus. Since the second apparatus was incompatible with monochromator usage, all the experiments with it involved the anticrossing carried by the $7d\,^1D$ emission.

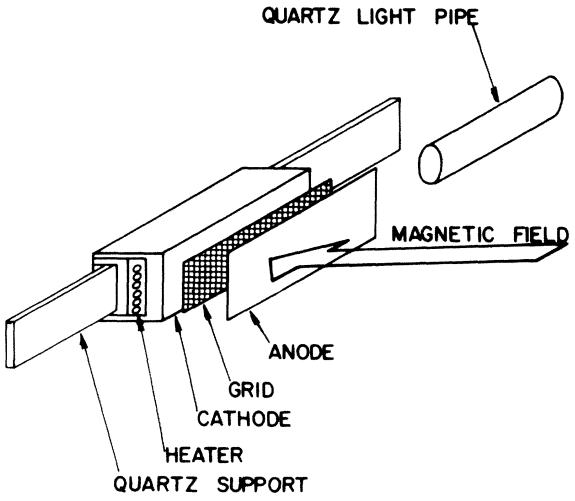

FIG. 3. New apparatus used to observe anticrossing in emission from the $7\,^1D$ state.

The following observations were obtained with this apparatus pictured in Fig. 3. The only signal observed was that assigned to the singlet-triplet anticrossing. The lines assigned to electric-field anticrossings were totally absent, presumably because the grid in the electron gun eliminated large space charges and the perpendicular electric fields associated with them. There did, however, appear to be a Stark effect caused by the parallel electric field between the grid and anode. The anticrossing line position was extrapolated to zero field by taking measurements with a 30–60-V differential between the grid and anode. The field position obtained in this way agreed within experimental error with that obtained from the zero current extrapolation in the MOMRIE apparatus.

IV. SPECTRAL ANALYSIS

A. Positions of anticrossings

As was noted in the experimental section, measurements of the line positions were taken at varying electron currents and electrode voltages. The results were then extrapolated to zero current or electric field conditions. It is these extrapolated values that we shall imply whenever we mention experimental-field positions. In both the $n=7$ and 8 case, separate measurements were made on the anticrossing curve carried by the ^1D light and the ^3D light. An example of these independent observations is shown for the $n=7$ states in Fig. 2. In all cases the measured positions of the anticrossing signals carried by the ^1D emission and the ^3D emission agree to well within experimental error. Hence we quote only one field (a simple average) for the anticrossing position. Likewise, the position of the $n=7$ anticrossing is an average for the two apparatuses.

These experimental field positions are given in Table V. The next column gives the corresponding zero magnetic-field separations assuming the value of g_e derived above. If we define the precise

TABLE V. Anticrossing field position and derived singlet-triplet intervals.

	Extrapolated field position (G)	Energy separation (MHz)	Singlet-triplet separation (MHz)
7*d*	9710 ± 20	13 624 ± 28	13 642 ± 28
8*d*	6750 ± 25	9470 ± 35	9483 ± 35

singlet-triplet interval as the energy difference, at zero electric and magnetic field, between the ^1D state and the center of gravity of the magnetic fine-structure components of the ^3D state, then the effects of E_2 must be eliminated from the experimental energy in column II. As will be shown below, the four anticrossings have essentially equal intensities. The shift in center position of the anticrossing is just the simple average of the last column of Table III. By subtracting these averages from the results in column II of Table IV, we obtain in Column III the singlet-triplet separation as defined above. It is probably worth noting that the corrections from E_2, while not negligible, are not large, and thus any small errors introduced by the approximations used to obtain E_2 should be unimportant.

B. Anticrossing width

As with the line position, the linewidth of which we will speak is the zero-current zero- (electric-) field limit. Also there is no notable variation between measurements of anticrossing width carried on the ^1D or ^3D line. The width in the MOMRIE apparatus was, however, slightly narrower than that recorded in the other apparatus, for which no good extrapolation to zero current and pressure could be obtained due to signal weakness. In fact, at the several lowest currents in the MOMRIE apparatus, the line appeared to have reached a constant "zero-field" limit. Thus only these low-current widths from the MOMRIE apparatus are used in this analysis.

These experimental full widths at half-height are given in gauss in Table VI. The corresponding widths in MHz are also given in Table VI. In order to interpret these widths it is well to look at Eq. (1), which gives the anticrossing signal. For given states, excitation, and detection systems, the full width $\Delta\nu$ at half-height is given by (in MHz)

$$\Delta\nu = \frac{2}{h}\left(4\,|\,V_{SM,TM'}\,|^2\,\frac{\tau_S\tau_T}{\bar{\tau}^2} + \hbar^2\bar{\tau}^{-2}\right)^{1/2}. \tag{20}$$

It may be noted from Table I that there are two distinct values of the perturbation $V_{SM,TM'}$ for the four distinct anticrossings. Thus all the lines need not be of the same intensity. In fact, if

$$4\,|\,V_{SM,TM'}\,|^2\,\frac{\tau_S\tau_T}{\bar{\tau}^2} \ll \hbar^2\bar{\tau}^{-2}, \tag{21}$$

then the intensity of two of the anticrossings will be 50% greater than the other two by Eq. (1). On the other hand, if

$$\hbar^2\bar{\tau}^{-2} \ll 4\,|\,V_{SM,TM'}\,|^2\,\frac{\tau_S\tau_T}{\bar{\tau}^2}, \tag{22}$$

then all of the intensities will be essentially equal.[27]

Fortunately, for the $n=7$ states Descoubes[22] has measured $\tau_S = 71 \pm 8$ nsec and $\tau_T = 190 \pm 70$ nsec. From these numbers we obtain $2(\bar{\tau})^{-1} \approx 3.0$ MHz, which is less than 1% of the observed width and about ten times smaller than the experimental error. Thus we see that inequality (22) applies; the anticrossing intensities are all the same, and the lifetime term makes a negligible contribution to the linewidth. Although no measurements on τ_S or τ_T are available for the $8\,^3D$ and ^1D states, they are probably slightly longer, and the same conclusions as for the 7 state must apply.

Thus we reach the conclusion that in both the $7d$ and $8d$ cases, we have four individual anticrossings separated by the intervals given in Table III. The intensities are all equal and the full widths at half-heights $\Delta\nu$ are given by

$$\Delta\nu = 4\mathfrak{A} f_M f_\tau, \tag{23}$$

where $f_\tau = (\tau_S\tau_T/\bar{\tau}^2)^{1/2}$ and $f_M = \sqrt{2}$ or $\sqrt{3}$, as given in Table I. With this information it is easy to construct on a computer the sum of four Lorentzians with the single variable parameter $\mathfrak{A} f_\tau$ to fit the observed width. Such a calculation was carried out on the same PDP-8E computer used to accumulate the data. The results are given in Table VI. For the $7d$ state, f_τ is 1.13 ± 0.10 from the data of Decoubes.[20] This leads directly to the value of $\mathfrak{A}$ listed in Table VI for the $7d$ state. As can be seen, the error in the determination of $\mathfrak{A}$ is about equally divided between the uncertainty in the linewidth and f_τ. For the $8d$ state, f_τ cannot be calculated as the lifetimes are unknown. However, they are almost certainly sufficiently close to the $7d$ values that f_τ for the $8d$ state would lie within the error bounds of the $7d$ value. Hence we adopt the $7d$ value and obtain the value of $\mathfrak{A}$ for the $8d$ state listed in Table VI.

V. DISCUSSION

The values obtained for the singlet-triplet separation can be compared with the previous best

TABLE VI. Value for full width at half-height for the anticrossing curves and the values of $\mathfrak{A}$, etc., derived therefrom.

	$7d$	$8d$
ΔH (G)	254 ± 20	180 ± 20
$\Delta\nu$ (MHz)	356 ± 28	253 ± 28
$\lvert\mathfrak{A}\rvert f_\tau$ (MHz)	56.6 ± 4.0	40.2 ± 4.0
$\lvert\mathfrak{A}\rvert$ (MHz) obs.	44.7 ± 6.8	32.3 ± 5.5
$\lvert\mathfrak{A}\rvert$ (MHz) theory	51.0	34.2

TABLE VII. Comparison of best theoretical calculations, optical observations, and the present results for the singlet-triplet interval. All results are in GHz.

	Theoretical		Optical	
	Parish and Mies[a]	Poe and Chang[b]	Martin[c]	Present Expt.
$7d$	42.8	13.52	14.7	13.64 ± .03
$8d$	29.3	...	10.8	9.48 ± .04

[a]Reference 26. [b]Reference 27. [c]Reference 14.

experimental values and the best theoretical calculations. Table VII shows that the best optical determinations overestimate the singlet-triplet separation by 1.15 and 1.32 GHz. Since the error in the optical values is roughly the same, it is possible that this error arises, not from errors in the individual measurements of the $7\,^{1,3}D$ and $8\,^{1,3}D$ to $2p\,^{1,3}P$ transition wavelengths, but from an error in the relative positions of the entire singlet and triplet manifold. This latter value is derived primarily from Herzberg's measurements[28] of the vacuum ultraviolet intercombination lines. Martin[16] states that it is unlikely that the intersystem connection is in error by more than 0.02 cm^{-1} (0.60 GHz); however, the consistent overestimation by ~1.2 GHz of the singlet-triplet intervals raises some doubt about the uncertainty in the intersystem connection. Clearly, anticrossing measurements between other singlet-triplet states would be needed to confirm this hypothesis.

The singlet-triplet intervals can also be compared to theoretical calculations. Calculations of absolute singlet and triplet energies for n values as high as 7 and 8 have been made by Parish and Mies.[29] For both the $7d$ and $8d$ states, their calculation seems to overestimate the actual intervals by roughly a factor of 3. Poe and Chang[30] have recently applied Brueckner-Goldstone perturbation theory to calculate electrostatic, exchange, and magnetic fine-structure intervals in the $n=7$ manifold. Their method has the advantage of calculating directly the desired intervals. Table VII shows that their calculation of the $7d$ singlet-triplet interval is quite close to the experimental value and is clearly better than that of Parish and Mies. This behavior is consistent with their excellent prediction of the electrostatic intervals measured by Wing and Lamb.[10]

The other important result of this experiment is the measurement of the spin-orbit coupling constant $\mathfrak{A}$ between the singlet and triplet states. Although this parameter is the fundamental measure of singlet-triplet interactions in any atomic or molecular system, we believe this is the first direct measurement of $\mathfrak{A}$ for any system.

Our values for $\mathfrak{A}$ are listed in Table VI and by comparison with Table II it can be seen that, for both the $7d$ and $8d$ states, $\mathfrak{A}$ is several times the diagonal spin-orbit coupling constant A. There are no detailed calculations of $\mathfrak{A}$ values for levels with $n>3$, but by $n=7$ and 8 the hydrogenic approximation of Bethe and Salpeter,[11] which was used to estimate various terms of E_2, would seem to be quite good. Although they applied their approximations only to calculate A, not $\mathfrak{A}$, their logic can be adopted to obtain a corresponding expression for $\mathfrak{A}$. Numerical evaluation of that expression leads to the values in the last row of Table VI. As can be seen, the predicted values for both the $7d$ and $8d$ states are equal to the observed ones, within experimental error. This seems a nice corroboration of the ability of the experiment to correctly determine the value of $\mathfrak{A}$.

The anticrossing method seems a powerful tool for studying singlet-triplet systems. We plan more measurements on lower rydberg states of the He atom to see if the optical intersystem connection is in error and in any case to improve its accuracy. While the lower n anticrossings will be broader and at higher field, Stark effects (the greatest experimental problem) are much smaller and lifetimes are better known. Also, it seems reasonable to extend the technique to simple molecular systems (e.g., H_2) to gain information about singlet-triplet intervals and relative manifold positions in molecular systems.

*Bell Laboratories summer visitor. Present address: Department of Physics, Morehouse College, Atlanta, Ga. 30314.

[1]R. W. Field, S. G. Tilford, R. A. Howard, and J. P. Simmons, J. Mol. Spectrosc. 44, 347 (1972).
[2]M. Levethal, Phys. Lett. 20, 625 (1966); T. G. Eck and R. J. Huff, Phys. Rev. Lett. 22, 319 (1969).
[3]H. J. Beyer and H. Kleinpoppen, J. Phys. B 4, L129

(1971); J. Phys. B 5, L12 (1972); H. J. Beyer, H. Kleinpoppen and J. M. Woolsey, Phys. Rev. Lett. 28, 263 (1972).
[4]H. Wieder and T. G. Eck, Phys. Rev. 153, 103 (1967).
[5]J. Von Neumann and E. Wigner, Phys. Z. 30, 467 (1929).
[6]P. A. Franken, Phys. Rev. 121, 508 (1961).
[7]T. G. Eck, L. L. Foldy, and H. Wieder, Phys. Rev. Lett. 10, 239 (1963).
[8]D. H. Levy, J. Chem. Phys. 56, 5493 (1972).
[9]T. A. Miller, J. Chem. Phys. 58, 2358 (1973).
[10]W. H. Wing and W. E. Lamb, Phys. Rev. Lett. 28, 265 (1972); At. Phys. 3, 119 (1973).
[11]G. Breit, Phys. Rev. 34, 553 (1929); Phys. Rev. 36, 383 (1930); Phys. Rev. 39, 616 (1932).
[12]H. A. Bethe and E. E. Salpeter, *Quantum Mechanics of One- and Two-Electron Atoms* (Springer-Verlag, Berlin, 1957).
[13]C. P. Slichter, *Principals of Magnetic Resonance* (Harper and Row, New York, 1963).
[14]E. U. Condon and G. H. Shortley, *The Theory of Atomic Spectra* (Cambridge U. P., Cambridge, England, 1967).
[15]G. Racah, Phys. Rev. 62, 438 (1942); 63, 367 (1943).
[16]W. C. Martin, J. Res. Nat. Bur. Stds. A 64, 19 (1960); J. Phys. Chem. Ref. Data 2, 257 (1973).
[17]S. A. Lewis, F. M. J. Pichanick, and V. W. Hughes, Phys. Rev. A 2, 86 (1970).
[18]T. A. Miller and R. S. Freund, Phys. Rev. A 4, 81 (1971).
[19]W. Lichten, Phys. Rev. 126, 1020 (1962).
[20]N. F. Ramsey, *Molecular Beams* (Oxford U. P., Oxford, England, 1956).
[21]T. A. Miller and R. S. Freund, Phys. Rev. A 5, 588 (1972).
[22]M. Maujean and J. P. Descoubes, C. R. Acad. Sci. Paris B 264, 1653 (1967) and J. P. Descoubes, *Physics of One- and Two-Electron Atoms* (North-Holland, Amsterdam, 1969), p. 341.
[23]H. G. Berry, J. L. Subtil, and M. Carre, J. Phys. Rad. 33, 947 (1972).
[24]W. E. Lamb, Phys. Rev. 85, 259 (1952).
[25]R. S. Freund and T. A. Miller, J. Chem. Phys. 56, 2211 (1972).
[26]R. S. Freund, Rev. Sci. Instrum. 41, 1213 (1970); D. MacNair, IEEE J. Quant. Electron. QE-5, 460 (1969).
[27]The conclusions rigorously rest on the assumption that $\rho^0_{S(T),M}$ is not dependent upon M, which is certainly not true, as all of our previous MOMRIE experiments rest on the difference in $\rho^0_{S(T),M}$ for various M values. However, the conclusions will still be valid as long as

$$|\rho^0_{S,M}-\rho^0_{T,M'}|\gg|\rho^0_{S(T),M''}-\rho^0_{S(T),M'''}|$$

for all M, M', M'', M'''. This assumption seems quite reasonable.
[28]G. Herzberg, Proc. Roy. Soc. Lond. A 248, 309 (1958).
[29]R. M. Parish and R. W. Mies, Phys. Rev. A 4, 2145 (1971).
[30]R. T. Poe and T. N. Chang, At. Phys. 3, 151 (1973).